1-1-2012

Room-temperature strong terahertz photon mixing in graphene

Sultan Shareef
University of Wollongong, sfs695@uow.edu.au

Yee Sin Ang
University of Wollongong, ysa190@uowmail.edu.au

Chao Zhang
University of Wollongong, czhang@uow.edu.au

Room-temperature strong terahertz photon mixing in graphene

Sultan Shareef, Yee Sin Ang, and Chao Zhang*

University of Wollongong, New South Wales 2522, Australia
**Corresponding author: czhang@uow.edu.au*

Received September 2, 2011; revised November 8, 2011; accepted November 11, 2011;
posted November 14, 2011 (Doc. ID 153799); published February 10, 2012

We demonstrate that single layer graphene exhibits a strong nonlinear photon-mixing effect in the terahertz frequency regime. Up to room temperature, the third-order nonlinear current in graphene grows rapidly with increasing temperature. The third-order nonlinear current can be as strong as the linear current under a moderate electric field strength of 10^4 V/cm. Because of the unique Dirac behavior of the graphene quasi-particles, low Fermi level and electron fillings optimizes the optical nonlinearity. Under a strong-field condition, the strong-field-induced Dirac fermion population redistribution and nonequilibrium carrier heating effects further amplify the optical nonlinearity of graphene. Our results suggest that doped graphene can potentially be utilized as a strong terahertz photon mixer in the room-temperature regime.

OCIS codes: 190.4380, 020.4180, 160.3918, 160.4236, 190.4720.

1. INTRODUCTION

Graphene is an monoatomically thin honeycomb nanostructure made up entirely of carbon atoms. Graphene is a zero-gap semiconductor. The loosely bound π electron forms a conduction band and a valence band that are degenerate at two inequivalent K and K' points in the first Brillouin zone. The degenerate point is commonly know as the *Dirac point*. Such nomenclature arises because the energy spectrum of the charge carriers at the vicinity of the Dirac points is equivalent to the linear energy dispersion of a massless ultrarelativistic fermions as described by Dirac's equation. Following its first successful isolation in 2004 [1], many fascinating and exotic phenomena have been observed [2]. This includes the unusually high carrier mobility [3,4], absence of carrier backscattering [5], the existence of a universal optical conductivity [6,7] and a finite conductivity in the limit of vanishing charge carrier concentration [8,9], a temperature-robust half-integer quantum hall effect [3,10–12], and strong suppression of weak localization in spite of graphene's low dimensionality [13], to name just a few of the many exciting properties found in graphene. Because of the unique Dirac point quasi-particle dynamics, graphene also serves as an ideal "scale-down" sandbox for the testing of high energy quantum physics [14].

Nonlinear optics plays a central role in the development of modern optics. Unfortunately, nonlinear optical effects in conventional semiconductors are usually minimal unless an extremely intense laser pulse is applied, and this greatly reduces the practicality of semiconductor-based devices. Recently, it has been demonstrated that the nonlinear optical response in graphene and several sister structures can be rather strong, especially in the important terahertz frequency regime [15–23]. For single layer graphene, strong terahertz interband [15] and intraband [16,17] nonlinear optical responses were theoretically predicted. Ishikawa has shown that, when both interband and and intraband processes are simultaneously considered, the optical nonlinearity is slightly reduced, but a strong terahertz response is still evident [18]. Experimentally, a strong nonlinear optical response in the visible and infrared regime [21,22], and frequency multiplication of millimeter waves is observed [23]. These studies open up the possibility of developing graphene-based devices for nonlinear optoelectronic and photonic applications. Such devices are much sought after not only because of graphene's unusually strong nonlinear response, but also because of the abundance of carbon atoms in nature and its waste-minimized bottom-up nanomanufacturing process.

The nonlinear intraband optical response of gapless graphene has been previously studied by Mikhailov *et al.*, who used the semiclassical Boltzmann transport equation for two limiting cases: (i) zero doping at finite temperature and (ii) finite doping at zero temperature [16,17]. The intermediate regime between (i) and (ii), i.e., doped graphene at finite temperature, is, however, left open and has not been reported so far. The nonlinear response in this intermediate regime is important since finite doping is usually present due to crystal imperfection and impurities, and the practical implementation of a graphene-based device requires finite temperature information. Furthermore, nonlinear response usually occurs under a strong external field. The strong-field-driven Dirac fermion (SDF) population redistribution, which is due to their externally perturbed dynamics and nonequilibrium carrier heating, becomes inevitable in the strong-field regime. The optical response of graphene with these strong-field effects considered has, however, not yet been reported, to the best of our knowledge. In this work, we fill in these gaps by constructing the full temperature spectrum of the nonlinear optical response of a finite-doped ($\mu \neq 0$) graphene single layer in both gapless and gapped cases under both weak-field and strong-field conditions. By directly decomposing the carrier dynamics into linear and nonlinear components when driven by an external AC electric field, we show that, for doped graphene, the third-order nonlinear optical response in the terahertz frequency regime easily dominates over the linear response with a moderate electric field strength of

10^4 V/cm and this nonlinear response is thermally enhanced up to room temperature. Interestingly, when strong-field effects are considered, the optical nonlinearity of graphene is further amplified and the electric field strength can be reduced to the order of 10^3 V/cm. This clearly indicates the potential of single layer graphene as a room-temperature terahertz-wave photon mixer.

2. THEORY

The effective Hamiltonian of graphene for a low energy carrier expanded around the K point is given by

$$\hat{\mathbf{H}} = v_F \begin{bmatrix} 0 & p_- \\ p_+ & 0 \end{bmatrix}, \tag{1}$$

where the Fermi velocity is $v_F = 3ta/2\hbar \approx 10^6$ m/s, $t \approx 3$ eV is the nearest-neighbor hopping bandwidth, $a \approx 0.142$ nm is the carbon–carbon distance, and $p_\pm = p_x \pm ip_y$. The energy eigenvalue of Eq. (1) gives rise to the linear energy dispersion $\varepsilon_s = sv_F p$, where $s = \pm 1$. This energy dispersion results in symmetric upper ($s = +1$) and lower ($s = -1$) Dirac cones, representing electrons and hole states, respectively, and is analogue to the charge conjugation symmetry in quantum electrodynamics. The velocity operator is given by $\hat{v} = \partial\hat{\mathbf{H}}/\partial p$. Following Feynman [24], we write the expectation value of $\hat{v}$ as $\langle \hat{v}_s \rangle = \partial\varepsilon_s/\partial p$. This gives velocity eigenvector $\mathbf{v}_s = sv_F\mathbf{p}/p$. We consider a time-dependent applied electric field in the form of

$$\mathbf{E}(\mathbf{r}, t) = \sum_\mu \mathbf{E}_\mu \exp\{i(\mathbf{q}_\mu \cdot \mathbf{r} - \omega_\mu t)\}, \tag{2}$$

where $\mathbf{E}_\mu$, $\mathbf{q}_\mu$, and ω_μ are the amplitude, wave vector, and frequency of μth wave of the electric field. Ignoring the weak magnetic component, the external field is minimally coupled to the quasi-particle by performing the substitution $\mathbf{p} \to \mathbf{p} - e\mathbf{A}(\mathbf{r}, t)$, where $\mathbf{E}(\mathbf{r}, t) = -\partial\mathbf{A}(\mathbf{r}, t)/\partial t$ and e is the electric charge. A straightforward expansion of $\mathbf{v}_s$ up to third order of the applied field, assuming $p \gg u$ where $\mathbf{u} = -e\mathbf{A}(\mathbf{r}, t)$, gives

$$\mathbf{v}_s^{(0)} = sv_F\left(\frac{\mathbf{p}}{p}\right), \tag{3}$$

$$\mathbf{v}_s^{(1)} = sv_F\left[\frac{\mathbf{u}}{p} - \frac{\mathbf{p}}{p}\left(\frac{\mathbf{p}\cdot\mathbf{u}}{p^2}\right)\right], \tag{4}$$

$$\mathbf{v}_s^{(2)} = -sv_F\left[\frac{\mathbf{p}}{2p}\left(\frac{u}{p}\right)^2 + \frac{\mathbf{u}}{p}\left(\frac{\mathbf{p}\cdot\mathbf{u}}{p^2}\right) + \frac{3\mathbf{p}}{2p}\left(\frac{\mathbf{p}\cdot\mathbf{u}}{p^2}\right)\right], \tag{5}$$

$$\mathbf{v}_s^{(3)} = sv_F\left[-\frac{1}{2}\frac{\mathbf{u}}{p}\left(\frac{u}{p}\right)^2 + \frac{3}{2}\frac{\mathbf{p}}{p}\left(\frac{u}{p}\right)^2\left(\frac{\mathbf{p}\cdot\mathbf{u}}{p^2}\right) + \frac{3}{2}\frac{\mathbf{u}}{p}\left(\frac{\mathbf{p}\cdot\mathbf{u}}{p^2}\right)^2 - \frac{5}{2}\frac{\mathbf{p}}{p}\left(\frac{\mathbf{p}\cdot\mathbf{u}}{p^2}\right)^3\right], \tag{6}$$

where $\mathbf{v}_s^{(i)}$ represents the ith-order velocity of graphene per spin and per valley degeneracy. The zero-order velocity is equal to the Fermi velocity v_F, which is consistent with the unperturbed case. Note that the velocities reverse the directions for opposite $s = \pm 1$ Dirac cones due to the particle–hole symmetry.

The ith-order current is given by

$$\mathbf{J}^{(i)} = e\sum_s \int_0^{2\pi} \int_{\mu-\varepsilon_{\rm ph}-k_BT}^{\Lambda} \mathrm{d}^2 p \mathbf{v}_s^{(i)} f(\varepsilon_s), \tag{7}$$

where $\varepsilon_{\rm ph}$ is the energy of the incoming photons, k_B is the Boltzmann constant, T is the temperature, and $f(\varepsilon_s)$ is the Fermi–Dirac distribution function. The integration cutoff Λ is equal to the Fermi-level μ at $T = 0$ K, and is arbitrarily set to a large value of 0.5 eV for $T > 0$ K and $\mu > 0$ numerical calculation. Up to room temperature, the Fermi–Dirac distribution terminates the momentum integration well before Λ and, hence, our choice of Λ is well justified. For $\mu < 0$, Λ terminates the momentum integration at $\mu + k_BT$ to avoid the low-momentum regime where $p \gg u$ fails. Deep charge carriers cannot respond to the external perturbation due to the unavailability of higher energy states. We qualitatively approximate this by choosing a lower momentum integration limit of $\mu - \varepsilon_s - k_BT$.

3. LINEAR OPTICAL RESPONSE

The linear current density for $\mu > \varepsilon_{\rm ph}$ at $T = 0$ K, including spin and valley degeneracy, is given by

$$\mathbf{J}_{T=0}^{(1)} = -i\frac{e^2}{\pi\hbar}\sum_\mu \mathbf{E}_\mu \exp\{i(\mathbf{q}_\mu \cdot \mathbf{r} - \omega_\mu t)\}. \tag{8}$$

Equation (8) corresponds to a linear conductivity of $\sigma_{T=0}^{(1)} = e^2/\pi\hbar$ and is in agreement with the linear conductivity calculated using the Kubo formula [8,9]. For $\mu < 0$, the current density reverses the direction since it is now contributed by $s = -1$ carriers. For $T > 0$ K, we obtain

$$\mathbf{J}_T^{(1)} = -i\frac{e^2}{\pi\hbar}\frac{k_BT}{\hbar\omega}\ln\left[1 + \exp\left(1 + \frac{\hbar\omega}{k_BT}\right)\right] \times \sum_\mu \mathbf{E}_\mu \exp\{i(\mathbf{q}_\mu \cdot \mathbf{r} - \omega_\mu t)\}, \tag{9}$$

which reduces to Eq. (8) in the limit of $T \to 0$.

4. NONLINEAR THREE-PHOTON MIXING

It is straightforward to show that the second-order velocity $\mathbf{v}_s^{(2)}$ does not generate any electric current due to the inversion symmetry of graphene. The third-order nonlinear current at $T = 0$ K is given by

$$\mathbf{J}_{T=0}^{(3)} = -is\frac{e^4v_F^2}{8\pi\hbar^2\mu}\sum_{\mu\nu\xi}\left(\frac{\varepsilon_{\mu\nu\xi}}{\mu - \varepsilon_{\mu\nu\xi}}\right)\frac{\mathbf{E}_\mu \cdot \mathbf{E}_\nu\mathbf{E}_\xi}{\omega_\mu\omega_\nu\omega_\xi} \times \exp\{i[(\mathbf{q}_\mu + \mathbf{q}_\nu + \mathbf{q}_\xi)\cdot\mathbf{r} - (\omega_\mu + \omega_\nu + \omega_\xi)t]\}, \tag{10}$$

where $s = +1$ (-1) for $\mu > 0$ ($\mu < 0$) and $\mu > \varepsilon_{\mu\nu\xi}$ where $\varepsilon_{\mu\nu\xi} = \varepsilon_\mu + \varepsilon_\nu + \varepsilon_\xi$ is the sum of three incoming photon energies. The magnitude of the zero temperature nonlinear current density is the same for electron filling ($\mu > 0$) and hole filling ($\mu < 0$) due to the up–down Dirac cone symmetry. At finite temperature, the nonlinear current density is obtained from

$$\mathbf{J}_T^{(3)} = -is\frac{e^4 v_F^2}{8\pi\hbar^2}\sum_{\mu\nu\xi}\frac{\mathbf{E}_\mu\cdot\mathbf{E}_\upsilon\mathbf{E}_\xi}{\omega_\mu\omega_\nu\omega_\xi}\int\frac{d\varepsilon_p}{\varepsilon_p^2}\frac{1}{1+\exp\left(\frac{\varepsilon_p-\mu}{k_BT}\right)}$$

$$\times\exp\{i[(\mathbf{q}_\mu+\mathbf{q}_\nu+\mathbf{q}_\xi)\cdot\mathbf{r}-(\omega_\mu+\omega_\nu+\omega_\xi)t]\}, \quad (11)$$

where, for simplicity, we have suppressed the integration limit. We see that μ plays an important role in the finite temperature current density of graphene. As shown in Eq. (10), smaller μ generates stronger nonlinear current. However, the assumption of $p \gg u$ in the derivation of the nonlinear velocities is no longer valid if μ is too small, since this will involve charge carriers with momentum comparable to u. For terahertz waves at room temperature, the range of $|\mu| \gtrsim 0.05$ eV will be adequate for $p \gg u$ to hold, and we choose $\mu = 60$ meV as the smallest Fermi level throughout this work. Experimentally, the Fermi level is continuously tunable up to $\pm(1\sim 2)$ eV by an external gate voltage [25] and, hence, our choice of μ is practically achievable.

The numerical result of Eq. (11) is shown in Figs. 1 and 2. We observe three important and unusual features in the nonlinear optical response: the third-order nonlinear response is (i) *thermally enhanced* up to room temperature, (ii) approximately *inversely proportional to* μ; and (iii) *asymmetric* between $\mu > 0$ and $\mu < 0$. Feature (i) is due to the thermal extension of the charge carrier lower limit $\mu - \varepsilon_{\mu\nu\lambda} - k_BT$ at higher temperature. A thermally created vacancy at a higher energy level allows more low-lying charge carriers to be excited and this amplifies the nonlinear current. However, it should be emphasized that the nonlinear current does not grow indefinitely with increasing temperature. At much higher temperature, the charge carriers in the opposite Dirac cone contribute to an opposite nonlinear current generation, which eventually reduces in the net nonlinear current. This reduction is not observed in our case due to the largeness of μ we have chosen, i.e., the nonlinear current is always contributed by charge carriers in only one Dirac cone. For feature (ii), a small μ results in nonlinear current contributed by low-momentum charge carriers and this leads to the stronger current density. The combine effect of (i) and (ii) causes the superlinear growth of nonlinear current at $\mu = 60$ meV and $T > 150$ K. Feature (iii) is explained by the finite temperature Dirac fermion population distribution in graphene. Consider that μ is in an arbitrary magnitude of $\mu = \mu_0$. Switching the Fermi level from $\mu = +\mu_0$ to $\mu = -\mu_0$ is essentially equivalent

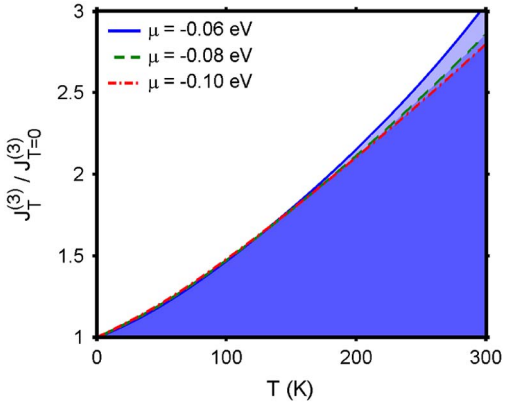

Fig. 1. (Color online) Temperature dependence of third-order nonlinear current density for $\mu < 0$ at $\omega = 1$ THz.

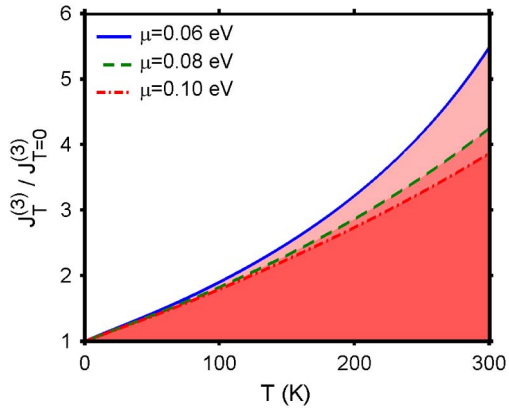

Fig. 2. (Color online) Temperature dependence of third-order nonlinear current density for $\mu > 0$ at $\omega = 1$ THz.

to the mirror reflection of the upper Dirac cone across the zero energy point into the lower Dirac cone. However, the Fermi–Dirac is not reflected, but is shifted downward by an amount of $2\mu_0$ and this breaks the overall up–down symmetry of the nonlinear currents at $\mu = \pm\mu_0$. When $\mu = +\mu_0$, a larger amount of low-lying $s = +1$ electrons becomes excitable at finite temperature and this significantly enhances the nonlinear current, while in the case of $\mu = -\mu_0$, a larger amount of deep $s = -1$ electrons becomes excitable and the nonlinear current enhancement is relatively weaker.

The strong nonlinear response of single layer graphene is not surprising if we consider the quasi-particle dynamics in graphene. The massless Dirac fermions around the K point are well described by a "pseudospin" Hamiltonian [Eq. (1)] and this pseudospin nature mimics the "real-spin" Rashba spin-orbit interaction (RSOI) term in two-dimensional electron gas (2DEG) confined in a quantum well structure, which has previously been shown to exhibit exceptionally strong nonlinear response [26]. In such a system, the enhanced nonlinearity is caused by the highly nonparabolic band structure induced by RSOI [27], while, in graphene, the linear (and, hence, highly nonparabolic) Dirac conic band structure results in the same enhanced optical nonlinearity. The linear optical response is, however, much smaller in graphene (linear conductivity of the order of quantum conductance e^2/h) and this gives rise to the relatively stronger optical nonlinearity in comparison to 2DEG with RSOI.

Two conclusions can be readily drawn from the above discussions. To achieve strong nonlinear optical effect in graphene, (i) small μ is preferred since low-lying electrons are strongly nonlinear, and (ii) electron filling $\mu > 0$ is preferred due to the broken Dirac fermion population symmetry at finite temperature.

We remark that the total optical conductivity should include both intraband and interband contributions. It can, however, be seen that σ_{inter} is forbidden in the few-terahertz regime due to the largeness of μ. By the virtue of momentum conservation, the requirement for the vertical interband transition can be written as $3\varepsilon_{\text{photon}} > 2\mu$ (where for simplicity, the three incoming photons are assumed to have the same energy $\varepsilon_{\text{photon}}$). For $\mu > 0.06$ eV, each photon has to exceed 0.04 eV, or frequency higher than 10 THz, for vertical interband transition to become possible and this is well beyond the few-terahertz regime considered here. Therefore, it is reasonable

to drop the σ_{inter} contribution and to consider σ_{intra} as the sole contributor to σ_{total}.

5. CRITICAL ELECTRIC FIELD AND PHOTON-MIXING EFFECT

We now discuss the electric field strength required to create a nonnegligible photon-mixing effect in graphene. We define a critical field strength such that $|\mathbf{J}^{(3)}|/|\mathbf{J}^{(1)}| = 1$. Combining Eq. (8) and Eq. (10), the $T = 0$ K critical field is given by

$$E_c(\omega, T = 0\text{ K}) = \frac{2\omega}{v_F}\left[\frac{2\mu}{e^2}\left(\frac{\mu}{3} - \hbar\omega\right)\right]^{1/2}, \tag{12}$$

where the two incident beams are assumed to have the same intensity and polarization. For $\omega = 1$ THz and $\mu = 0.1$ eV, the zero temperature critical field is approximately 10^4 V/cm. This electric field strength is rather moderate and is about 1 order of magnitude larger than the critical electric field of the three-photon nonlinear interband conductivity in intrinsic graphene [15]. At $T > 0$, the critical field is $E_c(\omega, T) = \beta E_c(\omega, T = 0\text{ K})$, where the dimensionless parameter β is defined as

$$\beta = \left\{\frac{k_B T}{\hbar\omega}\frac{\ln\left[1 + \exp\left(\frac{\hbar\omega}{k_B T} + 1\right)\right]}{|\mathbf{J}^{(3)}_{T>0}|/|\mathbf{J}^{(3)}_{T=0}|}\right\}^{1/2}, \tag{13}$$

and it describes the temperature dependence of the optical nonlinearity in graphene. The temperature dependence of β is plotted in Fig. 3. β exhibits contrasting behavior at the low- and high-temperature regimes. At the low-temperature regime, β increases with increasing temperature due to the stronger linear current. At higher temperature, the rate of increase of $J^{(3)}$ eventually exceeds $J^{(1)}$ and this leads to the peaking of β, and a further increment of temperature results in the lowering of β. For $\mu = 60$ meV, the β peaking is clearly observable at $T \approx 150$ K. The room-temperature E_c is approximately 10% lower than E_c at $T \approx 150$ K. For $\mu = 0.1$ eV and at room temperature, E_c is increased by about 60%, i.e., $E_c \approx 2 \times 10^4$ V/cm, and this is consistent with the experimental electric field strength where gigahertz waves mixing occurred [23].

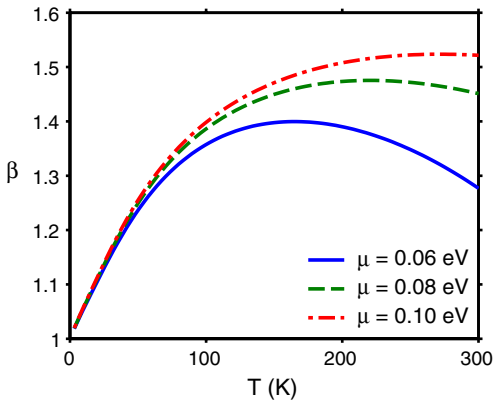

Fig. 3. (Color online) Temperature dependence of β at $\omega = 1$ THz. β exhibits contrasting behavior at the low- and high-temperature regimes.

The nonlinear optical absorption in graphene creates an oscillating current density $J^{(3)}$. This oscillation, in turn, induces an electromagnetic wave giving rise to the well-known four-wave-mixing phenomenon. The strong nonlinear current density in graphene immediately suggests the occurrence of a strong four-wave-mixing effect. The strength of the electric field $\mathbf{E}^{(3)}$ induced by the nonlinear mixing of $\omega_3 = 2\omega_1 \pm \omega_2$ can be estimated by solving Maxwell's inhomogeneous electromagnetic wave equation $\Box\mathbf{E}^{(3)} = (4\pi/c^2)\partial\mathbf{J}^{(3)}/\partial t$ where $\Box$ is the d'Alembert operator. At a distance far from the graphene single layer, the solution is approximately given by $\partial^2\mathbf{E}^{(3)}/\partial^2 t \propto \partial\mathbf{J}^{(3)}/\partial t$ and the corresponding third-order polarizability is given as

$$\chi^{(3)} = \frac{e^4 v_F^2}{8\pi\hbar^2\mu}\left(\frac{\hbar\omega_3}{\mu - \hbar\omega_3}\right)\frac{1}{\omega_2\omega_3}\left(\frac{1}{\omega_1\varepsilon_0}\right)^2. \tag{14}$$

6. OPTICAL RESPONSE OF HOT DIRAC FERMIONS

In the previous sections, the optical response is derived by assuming that the Dirac fermion population is well described by $f(\varepsilon_0)$, where $\varepsilon_0 = \mathbf{v}_s^{(0)} \cdot \mathbf{p}$ is the unperturbed linear energy spectrum. Under the strong-field condition, the simple assumption of $f(\varepsilon_0)$ is, however, no longer valid since the externally acquired dynamics $\Delta\varepsilon = (\mathbf{v}_s^{(1)} + \mathbf{v}_s^{(2)} + \mathbf{v}_s^{(3)}) \cdot \mathbf{p}$ is no longer negligible. This additional dynamics causes the Dirac fermions to redistribute themselves, resulting in a completely different distribution function of $f(\varepsilon_0) \to f(\varepsilon_0 + \Delta\varepsilon)$. In this section, we study the optical response of SDF in graphene with the strong-field-induced carrier population redistribution taken into account. It can be shown that a straightforward expansion of $f(\varepsilon_0 + \Delta\varepsilon) = \sum_{n=0}(\Delta\varepsilon)^n f_0^{(n)}/n!$ up to $n = 3$, where $f_0^{(n)}$ is the nth-order derivatives of $f(\varepsilon_0)$, yields $f(\varepsilon_0 + \Delta\varepsilon) = f(\varepsilon_0) + \Delta f_1 + \Delta f_2 + \Delta f_3$, where $\Delta f_1 = 0$, $\Delta f_2 = (\mathbf{v}_s^{(2)} \cdot \mathbf{p}) f_0^{(1)}$, and $\Delta f_3 = (\mathbf{v}_s^{(3)} \cdot \mathbf{p}) f_0^{(1)}$. By substituting $f(\varepsilon_0 + \Delta\varepsilon)$ into Eq. (7), the linear and nonlinear current densities in the strong-field regime can be written as

$$\mathbf{J}^{(1S)} = \mathbf{J}^{(1w)}, \tag{15}$$

$$\mathbf{J}^{(2S)} = 0, \tag{16}$$

$$\mathbf{J}^{(3S)} = \mathbf{J}^{(3w)} + \mathbf{J}^{(3')}, \tag{17}$$

where the superscripts (S) and (w) emphasize the optical response of SDFs and weak-field Dirac fermions, respectively. The consequences of Eqs. (15) and (16) are quite surprising: the linear and second-order nonlinear optical responses of graphene remain unchanged, although the whole SDF population has redistributed itself. This behavior can be understood by considering the nature of the strong-field-induced population redistribution phenomena. Such process is a description of how strongly the Dirac fermions respond to an external perturbation and the degree of redistribution depends on the coupling between the externally acquired dynamics and the unperturbed dynamics of Dirac fermions, i.e., $\mathbf{v}_{\text{external}} \cdot \mathbf{p}$. For a first-order response, it can be seen that the externally acquired first-order dynamics is completely decoupled from the unperturbed dynamics, i.e., $\mathbf{v}_s^{(1)} \cdot \mathbf{p} = 0$. As a result, this

orthogonality ensures that the linear response of graphene is always protected from the strong-field effect. For a second-order nonlinear response, the second-order coupling $\mathbf{v}_s^{(2)} \cdot \mathbf{p}$ is finite and one would intuitively expect a finite second-order current to occur. This is, however, not the case, as the additional second-order term vanishes after performing angular integration. In this case, although Dirac fermions are second-order perturbed and redistributed, the crystal itself remains unaffected and retains its inversion symmetry. Therefore, the second-order nonlinear response is still zero in strong-field regime.

The strong-field term $\mathbf{J}^{(3')}$ in Eq. (17) is given as

$$\mathbf{J}^{(3')} = \mathbf{J}^{(3')}_{T=0} \frac{\mu}{k_B T} \int \frac{\mathrm{d}p}{p} \frac{\exp\left(\frac{\varepsilon_0-\mu}{k_B T}\right)}{\left(\exp\left(\frac{\varepsilon_0-\mu}{k_B T}\right)+1\right)^2}, \tag{18}$$

where $\mathbf{J}^{(3')}_{T=0}$ is the $T = 0$ K results and is given by

$$\mathbf{J}^{(3')}_{T=0} = -is \sum_{\mu\nu\xi} \frac{\mathbf{E}_\mu \cdot \mathbf{E}_\upsilon \mathbf{E}_\xi}{\omega_\mu \omega_\nu \omega_\xi} \frac{e^4 v_F^2}{8\pi\hbar^2 \mu} \times \exp\{i[(\mathbf{q}_\mu + \mathbf{q}_\nu + \mathbf{q}_\xi)\cdot \mathbf{r} - (\omega_\mu + \omega_\nu + \omega_\xi)t]\}. \tag{19}$$

The critical electric field strength at $T = 0$ K is given as

$$E_c^{(S)}(T=0) = \frac{2\omega}{v_F}\left[\frac{2\hbar\omega}{e^2}(\mu - 3\hbar\omega)\right]. \tag{20}$$

For 1 THz and $\mu = 0.1$ eV, $E_c^{(S)}(T=0) = 3300$ V/cm and is 3 times smaller than that of the weak-field response. At finite temperature, we obtain $E_c^{(S)}(T) = \beta^{(S)}(T) E_c^{(S)}(T=0)$, where the dimensionless strong-field $\beta^{(S)}$ is given as

$$\beta^{(S)}(T) = \left\{\frac{k_B T}{\hbar\omega} \frac{\ln\left[1+\exp\left(\frac{\hbar\omega}{k_B T}+1\right)\right]}{|\mathbf{J}^{(3S)}_{T>0}|/|\mathbf{J}^{(3S)}_{T=0}|}\right\}^{1/2}. \tag{21}$$

It can be seen in Fig. 4 that $E_c^{(S)}$ is significantly lower than weak-field E_c over a wide temperature regime from $T =$ 0 K to $T = 600$ K. This indicates the stronger optical nonlinearity of SDFs in comparison to the usual Dirac fermions. The stronger optical nonlinearity of SDFs is due to the fact

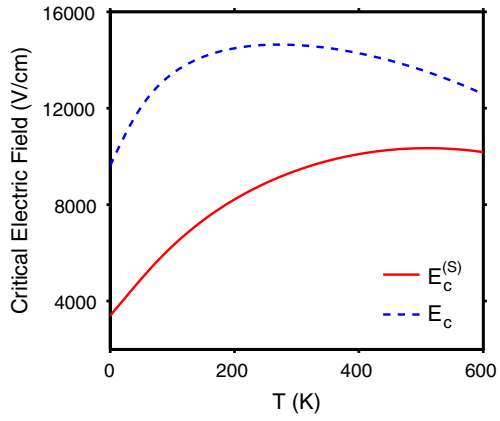

Fig. 4. (Color online) Critical field of $E_c^{(S)}$ at $\omega = 1$ THz and $\mu = 0.1$ eV. Weak-field critical field E_c is also shown.

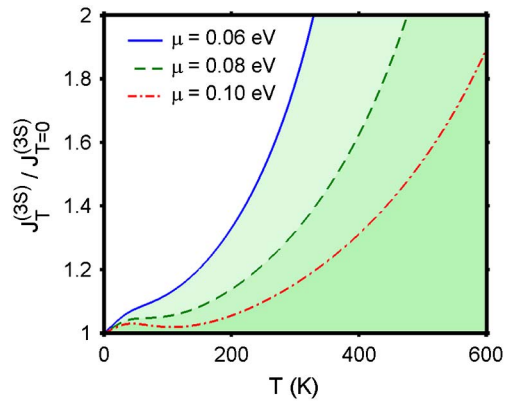

Fig. 5. (Color online) Temperature dependence of strong-field third-order nonlinear current density at $\omega = 1$ THz. Note that $T = T_{\text{lattice}}$ if nonequilibrium heating is ignored and $T = T_{\text{hot}}$ if nonequilibrium heating is considered. Since $T_{\text{hot}} > T_{\text{lattice}}$, the nonlinear optical response is significantly stronger if carrier heating is considered.

that the third-order nonlinear response is amplified by $\mathbf{J}^{(3')}$, while the linear response remains unchanged.

We now discuss the optical response due to nonequilibrium hot Dirac fermions in graphene. The hot Dirac fermions in graphene are short lived, especially in the case of high lattice temperature, where stronger electron–phonon coupling provides an efficient pathway for relaxation [28–30]. Under a weak-field condition, Dirac fermions rapidly thermalize themselves with the lattice, i.e., $T = T_{\text{lattice}}$. In a strong-field regime, the nonequilibrium heating of SDFs lifted the SDF temperature from the lattice temperature and, hence, the temperature terms in Eqs. (15) and (17) must be replaced by $T \to T_{\text{hot}}$, where T_{hot} is the hot SDF temperature and $T_{\text{hot}} > T_{\text{lattice}}$. For critical field variations between 10^3 V/cm and 10^4 V/cm, the hot SDF temperature reaches between $T_{\text{hot}} = 350$ K and $T_{\text{hot}} = 600$ K [31]. In contrast, equilibrium Dirac fermions are relatively "cold" since the lattice temperature in most of the practical application is up to only $T_{\text{lattice}} = 300$ K. It can be seen from Fig. 5 that the nonlinear current of hot SDFs in 350 K $< T_{\text{hot}} <$ 600 K is generally stronger than that of the cold equilibrium Dirac fermions where $T_{\text{lattice}} < 300$ K. Note that the temperature axis T in Fig. 5 has two alternative meanings: (i) without nonequilibrium SDF heating, $T = T_{\text{lattice}}$, and (ii) with nonequilibrium SDF heating, $T = T_{\text{hot}}$.

In summary, the optical response of graphene under the strong-field condition exhibits the following interesting behavior. (1) The linear and second-order nonlinear responses are well protected from the external field due to the unique Dirac fermion dynamics and the preservation of crystal inversion symmetry. (2) The third-order nonlinear optical response is enhanced by three distinct mechanisms: (i) the third-order response is intrinsically proportional to E^2, (ii) the SDF population redistribution creates an additional contribution to the third-order response, and (iii) the nonequilibrium heating raises the carrier temperature to $T_{\text{hot}} > T_{\text{lattice}}$ and further enhances the nonlinear current.

7. CONCLUSION

Finally, we point out several experiments that can potentially be used to verify our theoretical calculations. Several experimental works emphasizing the visible and near-infrared nonlinear optical response of graphene have been reported

recently [21,22,32]. Multiple-photon absorption/transmission experiments [22,32] can be repeated in the terahertz regime to qualitatively estimate the optical nonlinearity of graphene. The nonlinear wave-mixing effect can be more accurately quantified by irradiating a graphene sample with two waves at the terahertz level of frequencies ω_1 and ω_2, and selectively filtering the outgoing waves to determine the strength of the mixed wave $(2\omega_1 \pm \omega_2)$ [21]. The temperature dependence of the wave-mixing effect can be probed by performing these experiments under controlled temperature conditions.

In conclusion, we have presented a qualitative and quantitative analysis on the nonlinear effect and its temperature dependence in gapless and gapped graphene. In graphene, the nonlinear effect is approximately inversely proportional to the Fermi level and grows rapidly with temperature up to room temperature. The critical electric field required to generate a nonlinear effect comparable to the linear effect is in a rather moderate value of 10^4 V/cm even in room temperature. Under the strong-field condition, the Dirac fermion population redistribution and nonequilibrium carrier heating effects further enhance the optical nonlinearity of graphene. The strong and temperature-robust nonlinear optical nonlinearity suggests that graphene can potentially be an excellent candidate in nonlinear photon-mixing applications.

ACKNOWLEDGMENTS

This work is supported by the Australian Research Council (DP0879151).

REFERENCES

1. K. S. Novoselov, A. K. Geim, S. V. Morozov, D. Jiang, Y. Zhang, S. V. Dubonos, I. V. Dubonos, I. V. Grigorieva, and A. A. Firsov, "Electric field effect in atomically thin carbon films," Science **306**, 666–669 (2004).
2. A. K. Geim and K. S. Novoselov, "The rise of graphene," Nat. Mater. **6**, 183–191 (2007).
3. Y. Zhang, Y. Tan, H. L. Sormer, and P. Kim, "Experimental observation of the quantum Hall effect and Berry's phase in graphene," Nature **438**, 201–204 (2005).
4. K. I. Bolotin, K. J. Sikes, Z. Jiang, M. Klima, G. Fudenberg, J. Hone, P. Kim, and H. L. Stormer, "Ultrahigh electron mobility in suspended graphene," Solid State Commun. **146**, 351–355 (2008).
5. T. Ando, T. Nakanishi, and R. Saito, "Berry's phase and absence of back scattering in carbon nanotubes," J. Phys. Soc. Jpn. **67**, 2857–2862 (1998).
6. A. B. Kuzmenko, E. van Heumen, F. Carbone, and D. van der Marel, "Universal optical conductance of graphite," Phys. Rev. Lett. **100**, 117401 (2008).
7. K. F. Mak, M. Y. Sfeir, Y. Wu, C. H. Lui, J. A. Misewich, and T. F. Heinz, "Measurement of the optical conductivity of graphene," Phys. Rev. Lett. **101**, 196405 (2008).
8. A. W. W. Ludwig, M. P. A. Fisher, R. Shankar, and G. Grinstein, "Integer quantum Hall transition: an alternative approach and exact results," Phys. Rev. B **50**, 7526 (1994).
9. C. Zhang, L. Chen, and Z. Ma, "Orientation dependence of the optical spectra in graphene at high frequencies," Phys. Rev. B **77**, 241402(R)(2008).
10. Y. Zheng and T. Ando, "Hall conductivity of a two-dimensional graphite system," Phys. Rev. B **65**, 245420 (2002).
11. V. P. Gusynin and S. G. Sharapov, "Unconventional integer quantum Hall effect in graphene," Phys. Rev. Lett. **95**, 146801 (2005).
12. K. S. Novoselov, Z. Jiang, Y. Zhang, S. V. Morozov, H. L. Stormer, U. Zeitler, J. C. Maan, G. S. Boebinger, P. Kim, and A. K. Geim, "Room-temperature quantum Hall effect in graphene," Science **315**, 1379 (2007).
13. S. V. Morozov, K. S. Novoselov, M. I. Katsnelson, F. Schedin, L. A. Ponomarenko, D. Jiang, and A. K. Geim, "Strong suppression of weak localization in graphene," Phys. Rev. Lett. **97**, 016801 (2006).
14. K. S. Novoselov, A. K. Geim, S. V. Morozov, D. Jiang, M. I. Katsnelson, I. V. Grigorieva, S. V. Dubonos, and A. A. Firsov, "Two-dimensional gas of massless Dirac fermions in graphene," Nature **438**, 197–200 (2005).
15. A. R. Wright, X. G. Xu, J. C. Cao, and C. Zhang, "Strong nonlinear optical response of graphene in the terahertz regime," Appl. Phys. Lett. **95**, 072101 (2009).
16. S. A. Mikhailov, "Non-linear electromagnetic response of graphene," Europhys. Lett. **79**, 27002 (2007).
17. S. A. Mikhailov and K. Ziegler, "Nonlinear electromagnetic response of graphene: frequency multiplication and the self-consistent-field effects," J. Phys. Condens. Matter **20**, 384204 (2008).
18. K. L. Ishikawa, "Nonlinear optical response of graphene in time domain," Phys. Rev. B **82**, 201402(R) (2010).
19. Y. S. Ang, S. Sultan, and C. Zhang, "Nonlinear optical spectrum of bilayer graphene in the terahertz regime," Appl. Phys. Lett. **97**, 243110 (2010).
20. Y. S. Ang and C. Zhang, "Subgap optical conductivity in semi-hydrogenated graphene," Appl. Phys. Lett. **98**, 042107 (2011).
21. E. Hendry, P. J. Hale, J. Moger, and A. K. Savchenko, "Coherent nonlinear optical response of graphene," Phys. Rev. Lett. **105**, 097401 (2010).
22. J. Wang, Y. Hernandez, M. Lotya, J. N. Coleman, and W. J. Blau, "Broadband nonlinear optical response of graphene dispersions," Adv. Mater. **21**, 2430–2435 (2009).
23. M. Dragoman, D. Neculoiu, G. Deligeorgis, G. Konstantinidis, D. Dragoman, A. Cismaru, A. A. Muller, and R. Plana, "Millimeter-wave generation via frequency multiplication in graphene," Appl. Phys. Lett. **97**, 093101 (2010).
24. R. P. Feynman, "Forces in Molecules," Phys. Rev. **56**, 340–343 (1939).
25. C. Chen, C. Park, B. W. Boudouris, J. Horng, B. Geng, C. Girit, A. Zettl, M. F. Crommie, R. A. Segalman, S. G. Louie, and F. Wang, "Controlling inelastic light scattering quantum pathways in graphene," Nature **471**, 617–620 (2011).
26. F. Gao, G. Wang, and C. Zhang, "Strong photon-mixing of terahertz waves in semiconductor quantum wells induced by Rashba spin-orbit coupling," Nanotechnology **19**, 465401 (2008).
27. P. A. Wolff and G. A. Pearson, "Theory of optical mixing by mobile carriers in semiconductors," Phys. Rev. Lett. **17**, 1015–1017 (1966).
28. H. M. Dong, W. Xu, and R. B. Tan, "Temperature relaxation and energy loss of hot carriers in graphene," Solid State Commun. **150**, 1770–1773 (2010).
29. D. Sun, Z.-K. Wu, C. Divin, X. Li, C. Berger, W. A. Heer, P. N. First, and T. B. Norris, "Ultrafast relaxation of excited Dirac fermions in epitaxial graphene using optical differential transmission spectroscopy," Phys. Rev. Lett. **101**, 157402 (2008).
30. S. Butscher, F. Milde, M. Hirtschulz, E. Malic, and A. Knorr, "Hot electron relaxation and phonon dynamics in graphene," Appl. Phys. Lett. **91**, 203103 (2007).
31. W. S. Bao, S. Y. Liu, and X. L. Lei, "Hot-electron transport in graphene driven by intense terahertz fields," Phys. Lett. A **374**, 1266–1269 (2010).
32. G.-K. Lim, Z.-L. Chen, J. Clark, R. G. S. Goh, W.-H. Ng, H.-W. Tan, R. H. Friend, P. K. H. Ho, and L.-L. Chua, "Giant broadband nonlinear optical absorption response in dispersed graphene single sheets," Nat. Photon. **5**, 554–560 (2011).